Ligand-mediated protein degradation reveals functional conservation among sequence variants of the CUL4-type E3 ligase substrate receptor cereblon

Received for publication, September 13, 2017, and in revised form, February 15, 2018 Published, Papers in Press, February 15, 2018, DOI 10.1074/jbc.M117.816868

Afua A. Akuffo[‡§1], Aileen Y. Alontaga[‡1], Rainer Metcalf[¶1], Matthew S. Beatty[‡], Andreas Becker[‖], Jessica M. McDaniel[‡2], Rebecca S. Hesterberg[‡§], William E. Goodheart[‡], Steven Gunawan[**], Muhammad Ayaz[**], Yan Yang[‖], Md Rezaul Karim[**], Morgan E. Orobello[‡], Kenyon Daniel[¶], Wayne Guida[¶], Jeffrey A. Yoder[‡‡], Anjali M. Rajadhyaksha[§§], Ernst Schönbrunn[**], Harshani R. Lawrence[‖], Nicholas J. Lawrence[1], and Pearlie K. Epling-Burnette[‡1,3]**

From the [‡]Department of Immunology, the [‖]Chemical Biology Core, and the [**]Department of Drug Discovery, Moffitt Cancer Center and Research Institute, Tampa, Florida 33612, the [¶]Department of Chemistry and the [§]Cancer Biology Ph.D. Program, University of South Florida, Tampa, Florida 33612, the [‡‡]Department of Molecular Biomedical Sciences, College of Veterinary Medicine, North Carolina State University, Raleigh, North Carolina 27607, and [§§]Pediatric Neurology, Pediatrics, Brain and Mind Research Institute, Graduate Program in Neuroscience, Weill Cornell Medicine, Molecular and Developmental Neuroscience Laboratory, New York, New York 10065

Edited by George N. DeMartino

Upon binding to thalidomide and other immunomodulatory drugs, the E3 ligase substrate receptor cereblon (CRBN) promotes proteosomal destruction by engaging the DDB1–CUL4A–Roc1–RBX1 E3 ubiquitin ligase in human cells but not in mouse cells, suggesting that sequence variations in CRBN may cause its inactivation. Therapeutically, CRBN engagers have the potential for broad applications in cancer and immune therapy by specifically reducing protein expression through targeted ubiquitin-mediated degradation. To examine the effects of defined sequence changes on CRBN's activity, we performed a comprehensive study using complementary theoretical, biophysical, and biological assays aimed at understanding CRBN's nonprimate sequence variations. With a series of recombinant thalidomide-binding domain (TBD) proteins, we show that CRBN sequence variants retain their drug-binding properties to both classical immunomodulatory drugs and dBET1, a chemical compound and targeting ligand designed to degrade bromodomain-containing 4 (BRD4) via a CRBN-dependent mechanism. We further show that dBET1 stimulates CRBN's E3 ubiquitin–conjugating function and degrades BRD4 in both mouse and human cells. This insight paves the way for studies of CRBN-dependent proteasome-targeting molecules in nonprimate models and provides a new understanding of CRBN's substrate-recruiting function.

Cereblon (CRBN)[4] binds to thalidomide and other immunomodulatory drugs, including lenalidomide (Len) and pomalidomide (Pom), and is one of many DDB1 and CUL4-associated factors (DCAFs) that target specific protein substrates for ubiquitylation and proteasome-mediated degradation by the DDB1–CUL4A–Roc1–RBX1 E3 ubiquitin ligase complex (Fig. S1*A*) (1–3). Despite their teratogenic properties (4), immunomodulatory compounds have antineoplastic activity in multiple myeloma (5), myelodysplastic syndrome (MDS) associated with a somatically acquired deletion in chromosome 5 (del(5q) MDS) (6), and B cell malignancies (7–9) based on the substrates that are selected for proteosomal destruction by the bridging actions of these small molecules (Fig. S1*A*) (1, 2, 10–13). Len, Pom, and a newer derivative CC-122 (avadomide) (14) also potentiate the activation of T cells. Although this function has been studied less thoroughly, it is thought that the drug-induced proteosome-mediated degradation of transcriptional repressors of T cells, Ikaros and Aiolos, may be necessary for this response in addition to their defined role in antineoplastic activity (Fig. S1*A*) (15–17). Unlike human cells, mouse cells are resistant to these compounds, including antiproliferative multiple myeloma (18) and thalidomide-associated teratogenicity (19). Whereas the overall amino acid sequence of mouse CRBN is highly conserved (Fig. S1*B*), and it forms the DDB1 interaction (3), minor species–related sequence variations in the thalidomide-binding domain (TBD) of CRBN are thought to lead to nonconserved drug binding or altered E3 ligase recruitment functions. A single amino acid substitution, Val-388, which is

This work was supported through a Research Agreement with Celgene Corp. J. M. M. is currently a salaried employee of Celgene Corporation but was a graduate student in the Cancer Biology Ph.D. program at the time of this study. Dr. N. Lawrence and the Moffitt Cancer Center have received payment from licensing unrelated technology to Celgene and have appropriate conflict-of-interest management plans.

This article contains Figs. S1–S7 and Tables S1–S4.

[1] These authors contributed equally to this work.

[2] Present address: Celgene Corp., 556 Morris Ave., Summit, NJ 07901.

[3] To whom correspondence should be addressed: Dept. of Immunology, SRB 23033 Moffitt Cancer Center and Research Institute, Tampa, FL 33612. Tel.: 813-745-6177; Fax: 813-745-3829; E-mail: Pearlie.Burnette@moffitt.org.

[4] The abbreviations used are: CRBN, cereblon; hCRBN, human CRBN; mCRBN, mouse CRBN; gCRBN, chicken CRBN; Len, lenalidomide; Pom, pomalidomide; MDS, myelodysplastic syndrome; TBD, thalidomide-binding domain; BET, bromodomain and extraterminal domain; PROTAC, proteolysis targeting chimera; TCR, T-cell receptor; RMSD, root mean square deviation; MD, molecular dynamics; DDB1, DNA damage–binding protein 1; IFD, induced-fit docking; IF, intrinsic tryptophan fluorescence assay; ITC, isothermal titration calorimetry; CTV, cell trace violet; TCEP, tris(2-carboxyethyl)phosphine.

changed to isoleucine in mouse (Ile-391), has been reported to render mouse CRBN unable to degrade Ikaros, Aiolos, and CK1α binding through a β-hairpin–loop motif that is recognized only when CRBN is complexed with the immunomodulatory drugs (20). Therefore, a dysfunctional drug-induced substrate requirement possibly mediates drug resistance (20). Thus far, conservation of mouse CRBN's E3 ubiquitin–ligating function has not been definitely shown due to this loss of function, as the native ligands that are regulated through this pathway are poorly defined. Moreover, drug-binding affinity due to the V388I variant has not been studied in detail. A better understanding of this defect is important for future drug discovery efforts aimed at controlling intracellular protein degradation and understanding CRBN's endogenous role as an E3 ubiquitin ligase substrate receptor.

Here, we focused our analysis on nonprimate CRBN. Using drug binding assays to several CRBN sequence variants, we investigate whether these structural changes are likely to result in functional inactivation. We focused on CRBN's substrate recruiting function in mouse and human T cells, as this is poorly studied and important for defining applications in immune therapy. Both the Bradner and Crews laboratories conjugated JQ1, an established chemical inhibitor of bromodomain and extraterminal domain (BET) family members, to a thalidomide analog to promote the CRBN-dependent degradation of BRD4 (21, 22) Linkage of the BET-binding ligand (JQ1 or OTX-015) to an IMiD redirects CRBN-E3 ligase activity toward BRD4, allowing for analysis of different substrates through a similar TBD-dependent mechanism (Fig. S1). Moreover, the E3 ubiquitin protein–targeting approach, coined proteolysis targeting chimera (PROTAC) (23–25), may be broadly applied clinically and experimentally to study the function of proteins that are difficult to target and in cells that are insensitive to genome editing techniques. Here, we use a PROTAC probe to investigate cellular engagement of an immunomodulatory drug with mouse CRBN. Collectively, our findings are important to understand sequence variants of CRBN and provide the first investigation of the E3 ubiquitin ligase substrate-conjugating function of CRBN in a nonprimate vertebrate model.

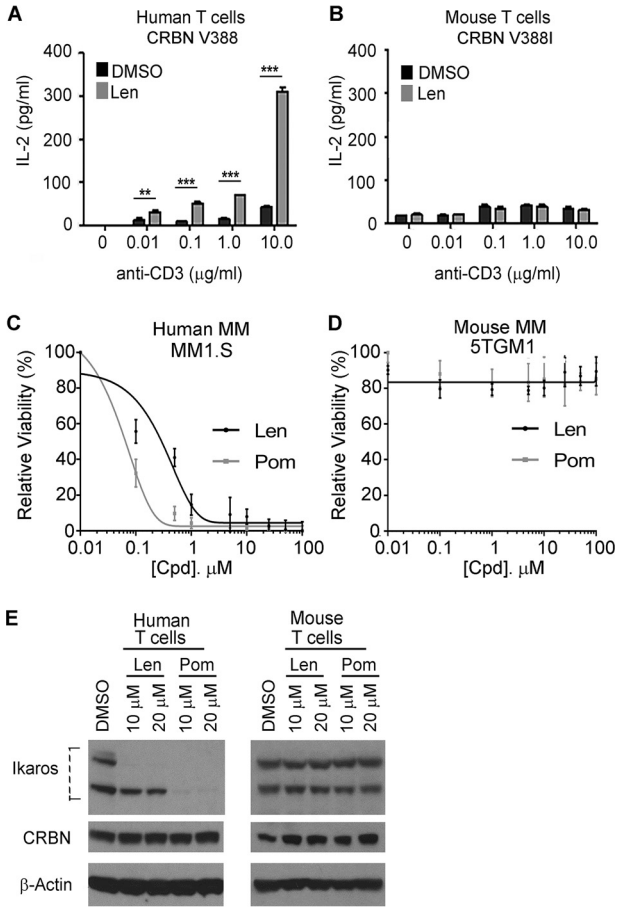

Figure 1. Mouse cells are resistant to immunomodulatory drugs. Shown are T cells purified from healthy donor peripheral blood mononuclear cells (*A*) or from mouse spleens of C57BL/6j mice (*B*) and stimulated in the presence of increasing concentrations of anti-CD3ϵ antibody in the presence of 10 μM Len or vehicle control (DMSO) without anti-CD28. IL-2 production was determined from the culture supernatant by ELISA. The human MM1.S (*C*) or mouse 5TGM1 (*D*) multiple myeloma cells were cultured for 7 days with increasing concentrations of Len, Pom, and vehicle (DMSO). Percentage relative cell viability is shown. *E*, Western blot analysis of Ikaros, CRBN, and β-actin (loading control) in human and mouse T cells stimulated with anti-CD3ϵ 5 μg/ml + 1 μg/ml anti-CD28 antibody for 24 h with DMSO and 10 and 20 μM lenalidomide and pomalidomide. Results are representative of three independent experiments. Statistical analysis was conducted using ANOVA, followed by Dunnett's multiple comparison test. *, $p < 0.05$; ***, $p < 0.001$ (see also Fig. S2). *Error bars*, S.D.

Results

Resistance of mouse cells to immunomodulatory compounds

Comparative analyses of CRBN sequences from representative vertebrate species revealed that Ile-391 is conserved among many nonprimate mammals (mouse, rat, dog, manatee, and opossum), birds (chicken and zebra finch), reptiles (alligator), amphibians (*Xenopus*), bony fish (zebrafish and spotted gar), and cartilaginous fish (whale shark) (Fig. S1*B*) (26). Interestingly, both chicken and zebrafish are susceptible to thalidomide-induced teratogenicity despite expressing the Ile-391 variant (3). In contrast, Val-388 is present in all examined primate sequences (human, chimpanzee, gorilla, orangutan, gibbon, macaque, baboon, green monkey, squirrel monkey, marmoset, tarsier, and Sunda flying lemur) with the exception of the gray mouse lemur sequence, which encodes Ile in this position (Fig. S1*B*). Therefore, Val-388 is a recently derived feature present in most primates.

Immunomodulatory drug–induced ubiquitin-mediated degradation of Ikaros and Aiolos (encoded by *IKZF1* and *IKZF3*, respectively) (1, 27) appears sufficient to augment IL-2 production by T cells (28) in the absence and presence of anti-CD28 co-stimulation (15, 29, 30). In Len-treated human T cells stimulated with anti-CD3ϵ antibody to cross-link the T-cell receptor (TCR), levels of *IL2* mRNA (Fig. S2*A*) and protein (Fig. S2*B*) were significantly increased relative to DMSO (vehicle)-treated cells. Comparing purified human (Fig. 1*A*) and mouse T cells (Fig. 1*B*) pretreated with vehicle or 10 μM Len, only human T cells displayed the expected Len-induced increase in IL-2 when stimulated in the absence (Fig. 1, *A* and *B*) or presence (Fig. S2, *C* and *D*) of anti-CD28 antibody using doses of anti-CD3ϵ that ranged from 0.01 to 10 μM.

Thalidomide, Len, and Pom's antiproliferative effects in multiple myeloma cell lines also reportedly differ based on the presence of mouse CRBN (18, 20, 31). In U266 (Table S1), H929

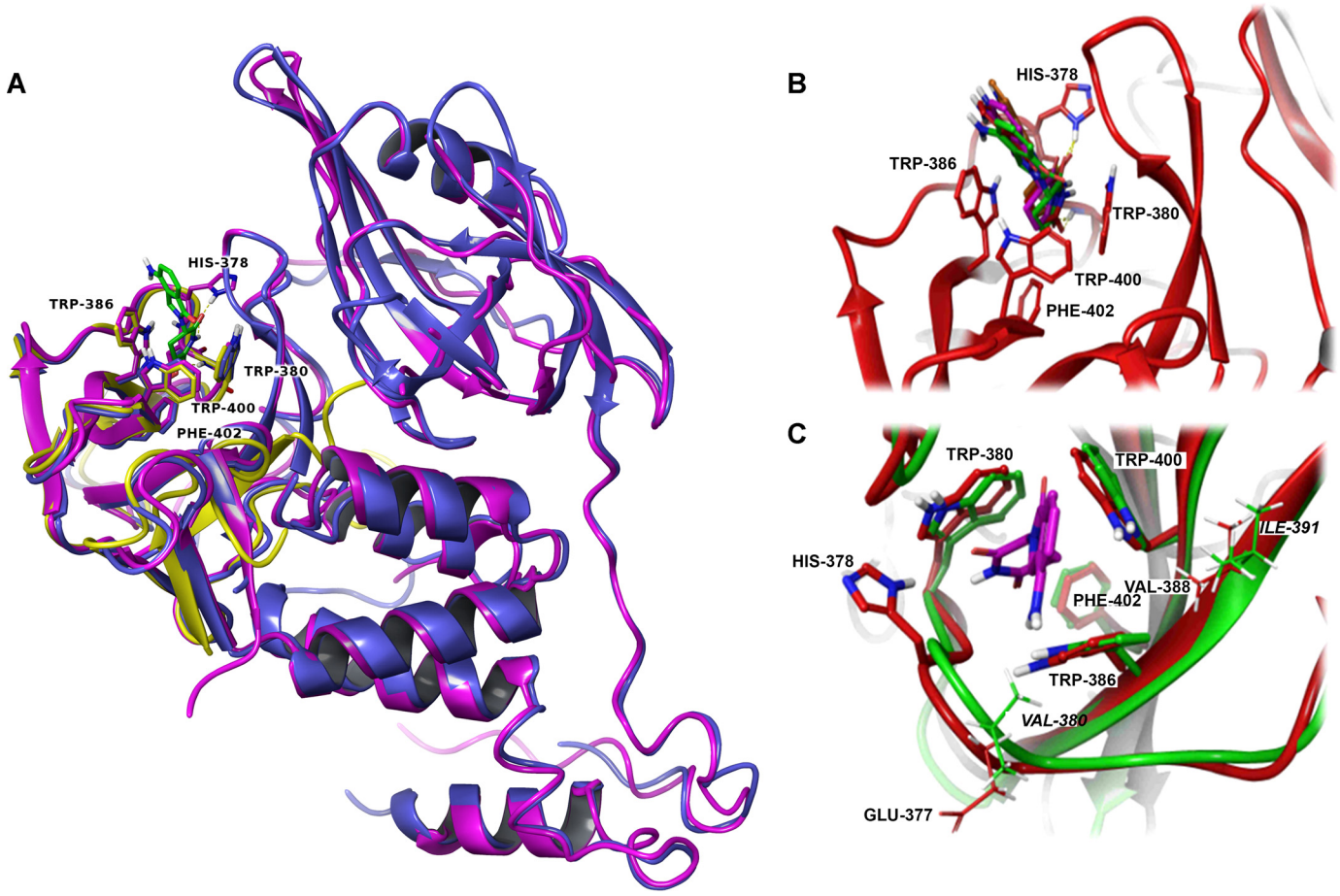

Figure 2. Structure of cereblon is conserved across different species. *A*, *ribbon overlays* of human (*purple*; PDB code 4TZ4) and chicken (*blue*; PDB code 4CI2) X-ray crystal structures and post-MD structure of mouse (*yellow*; PDB code 4TZ4) cereblon. Human immunomodulatory drug–binding site residues His-378, Trp-380, Trp-386, and Phe-402 and ligands thalidomide (*yellow*), lenalidomide (*green*) and pomalidomide (*blue*) are shown for reference. *B*, superposition of ligand poses of lenalidomide for the post-MD equilibrated systems of the CRBN thalidomide-binding site after IFD for hCRBN (*red*), hmCRBN (*green*), and gCRBN (*orange*), shown with the post-MD equilibrated protein structure of hCRBN (*red*) for reference. *C*, overlays of human and mouse cereblon show nonconserved residues Ile-391 for mCRBN (human Val-388), Val-380 for mCRBN (human Glu-377) (mouse shown in *italic type*) (see also Fig. S3).

(Table S1), and MM1.S multiple myeloma cell lines (Fig. 1*C* and Table S1), the antiproliferative effects (IC_{50} values) of Pom ranged from 0.05 to 0.51 μM, and for Len, they ranged from 1.5 to 10 μM. In contrast, the mouse multiple myeloma cell line 5TGM1 was resistant to immunomodulatory drugs (Fig. 2*D* and Table S1). Further, Ikaros protein expression was unaffected in primary mouse T cells *versus* almost completely depleted in human cells (Fig. 1*E*), as predicted from previous structural and functional studies in multiple myeloma cell lines and in the Ba/F3 mouse lymphoma cell line (13, 20).

Thalidomide-binding domain of CRBN has a conserved immunomodulatory compound–binding motif

Next, the sequence variants of CRBN were studied in more detail. Based on crystal structures, immunomodulatory compounds bind to a conserved pocket within the C-terminal TBD of CRBN (Fig. S1 and Fig. 2*A*) (32, 33). These interactions are governed by hydrogen bonding, aromatic quadrupole, and van der Waals interactions. Analysis of the X-ray crystal structures of CRBN (human (hCRBN), mouse (mCRBN), and chicken (gCRBN)) in complex with thalidomide, Len, and Pom, respectively (Fig. 2*A*), shows negligible variations of root mean square deviation (RMSD) between the inhibitor poses. Thus, an in-depth theoretical investigation of the molecular binding mechanics of immunomodulatory compounds in complex with CRBN was conducted to explore possible differences in drug interactions between mouse and human CRBN caused by induced fit or protein flexibility.

For molecular dynamics (MD), simulations of the crystal structures of hCRBN (Protein Data Bank (PDB) code 4TZ4) (32) and gCRBN (PDB codes 4CI1, 4CI2, and 4CI3) (32) in complex with DDB1 were used. The crystal structure of mCRBN (PDB codes 4TZC and 4TZU) (33) is monomeric and truncated to contain only the TBD (108 defined residues compared with 380 defined residues for hCRBN and gCRBN) and is not suitable for computational modeling. The amino acid differences in mouse CRBN (when compared with human CRBN) include C366S, E377V (which may be specific to rodents), and V388I (Fig. 1*B*). Therefore, to further increase sampling and determine any structural dependence on these residues, the original hCRBN sequence of the equilibrated representative structure was mutated to the mouse sequence. The mCRBN analog and hmCRBN hybrid developed from the hCRBN system is capable of reproducing the crystal ligand poses of mCRBN (PDB codes 4TZC and 4TZU) with minimal conformational deviation (Fig.

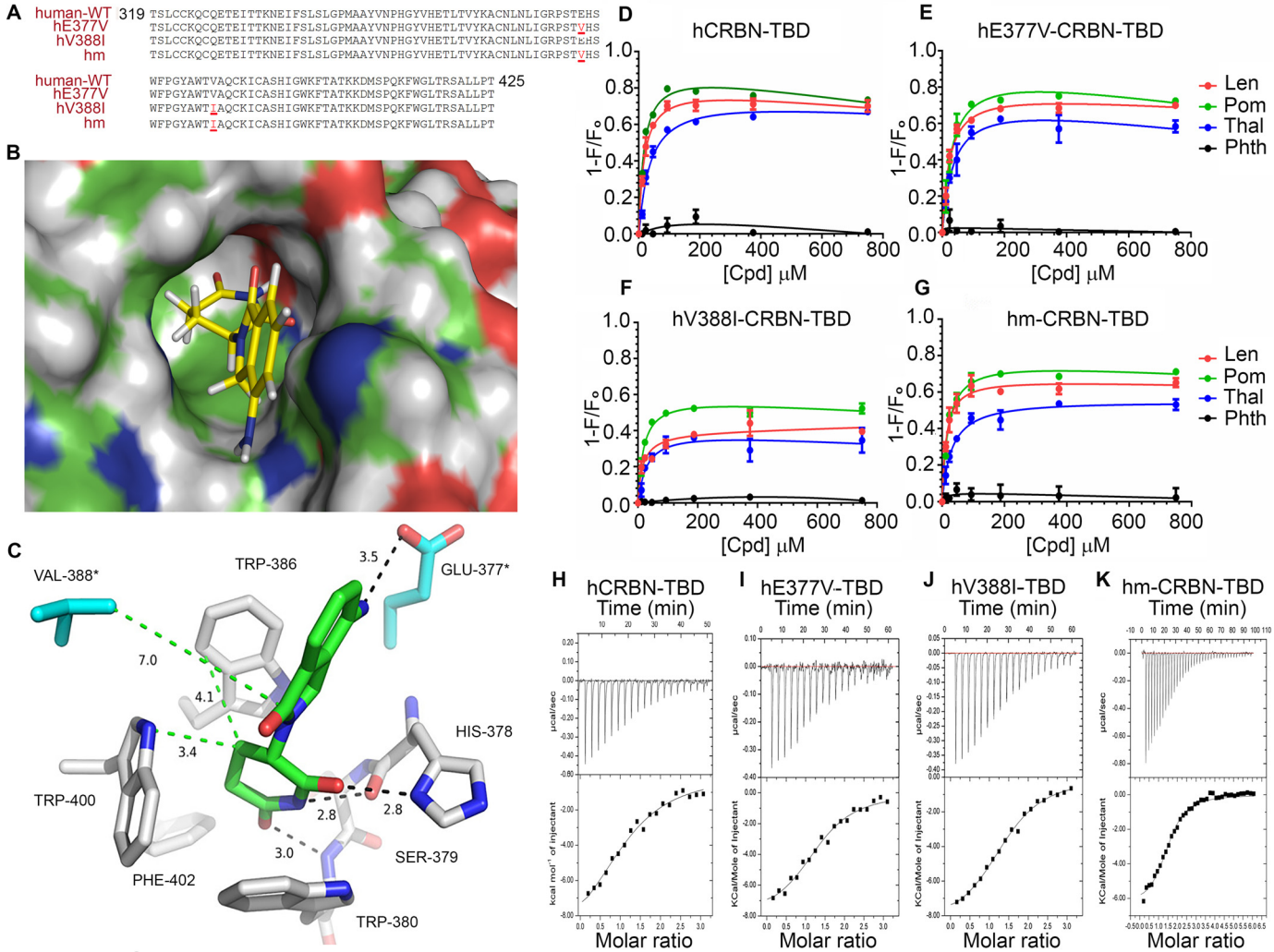

Figure 3. Human and mouse CRBN binds IMiDs with similar affinities. *A*, sequence alignment of human CRBN and human-to-mouse mutations. Mutations introduced to convert human to mouse are *highlighted* in *red*. *B*, IMiD interaction in the hydrophobic binding pocket. *C*, lenalidomide (*green*) interacts with the TBD site (*gray*) through hydrogen bonds (*dashed black lines*) with backbone residues His-378, Ser-379, and Trp-380 van der Waals interactions (*dashed green lines*) that occur with the side chains of Trp-380, Trp-386, Trp-400, and Phe-402 (mouse: Trp-383, Trp-389, Trp-403, and Phe-405). The two residues differing between the human and the mouse proteins are *highlighted* in *cyan*. Shown are titration of human TBD WT (*D*), E377V (*E*), V388I (*F*), and E377V/V388I (hmCRBN–TBD) (*G*) to lenalidomide (*red*), pomalidomide (*green*), thalidomide (*blue*), and phthalimide (*black*) by intrinsic tryptophan fluorescence assay. K_D values were calculated based on the magnitude of fluorescence differences ($1 - F/F_0$). *H–K*, isothermal titration calorimetry saturation curve using Len for human TBD and mutants (see also Figs. S3–S5 and Table 1). *Error bars*, S.D.

2*C*) and was used for modeling purposes. Binding modes do not appear to differ between models and compounds, as there are no significant differences in RMSD calculations between X-ray crystal binding poses (Table S2) and post-MD equilibrated models (Figs. 2, *B* and *C*). Induced-fit docking (IFD) also predicts no observable difference in binding affinity between models and compounds (Table S2). All poses are within 1.8 Å RMSD, which is the expected threshold for the IFD protocol (34).

Although Val-388 of hCRBN recruits Ikaros, Aiolos, and CK1α upon immunomodulatory compound binding (20), the side chain is >6 Å away from the immunomodulatory drug, and it is thus unlikely to alter binding affinity to the drugs. The second distinct amino acid is Glu-377, which in the mouse is Val-380 and could establish a weak hydrogen bond with Len's amino group. However, hydrogen-bond analysis (Fig. S3) of MD simulations suggests that minimal interaction occurs between this residue and bound immunomodulatory drugs, mainly due to the backbone dihedral strain tending to force the charged carboxyl moiety away from the binding site.

Immunomodulatory compound binding is conserved in CRBN sequence variants

Amino acids in mouse CRBN–TBD at Val-380 (equivalent to human Glu-377) and Ile-391 (equivalent to human Val-388) (Fig. 3, *A–C*) appear to have no relevance in the structure or corresponding immunomodulatory drug–binding interaction based on theoretical modeling. To test the effects of these two nonconserved amino acids on binding affinity, the recombinant human TBD motif (residues 319–425) was expressed in *Escherichia coli* (Fig. S4*A*) and mutated to the mouse variants (Fig. 3, *A–C*). Immunomodulatory drug binding was then analyzed using two distinct assays, an intrinsic tryptophan fluorescence assay (IF) (Fig. 3, *D–G*) and isothermal titration calorimetry (ITC) (Fig. 3, *H–K*). The C366S amino acid mutation was not studied in binding assays, as it is more than 20 Å away from the

Table 1
Binding affinity (K_D, [μM]) of immunomodulatory compounds to WT and mutant human CRBN-TBD determined using ITC and fluorescence intensity assay
Data represent mean ± S.D. FI, fluorescence intensity; NB, non-binding; NP, not performed.

TBD	Assay	K_D				
		Lenalidomide	Pomalidomide	Thalidomide	Phthalimide	dBET1
hCRBN	ITC	11 ± 3	16 ± 4	65 ± 40	NB	NP
	FI	13 ± 2	16 ± 3	38 ± 12	NB	16 ± 2
hCRBN-H378A	ITC	22 ± 3	35 ± 8	37.4 ± 10	NB	NP
	FI	27 ± 4	22 ± 6	74 ± 20	NB	NP
hCRBN-W380A	ITC	NB	NB	NB	NB	NP
	FI	NB	NB	NB	NB	NP
hCRBN-E377V	ITC	9.6 ± 2	35 ± 9	97 ± 100	NB	NP
	FI	22 ± 2	30 ± 7	36 ± 8	NB	NP
hCRBN-V388I	ITC	10 ± 1	28 ± 7	43 ± 20	NB	NP
	FI	14 ± 4	16 ± 4	39 ± 1	NB	13 ± 2
hmCRBN-E377V/V388I	ITC	14 ± 2	8 ± 2	34 ± 2	NB	NP
	FI	13 ± 3	19 ± 4	30 ± 8	NB	NP

immunomodulatory drug–binding pocket. The TBD is structurally stabilized by four cysteine residues (Cys-323, Cys-326, Cys-391, and Cys-394) that coordinate a single zinc ion (32, 33), located ~18 Å from the drug-interacting site. To gain insights into the role of zinc, mutations in the C*XX*C domain of the TBD were also generated. Mutating any of the cysteine residues resulted in insoluble protein that aggregated in inclusion bodies (Fig. S4*B*). This is indicative of misfolding due to loss of Zn^{2+} ion coordination. To rule out improper folding or destabilization, a zincon assay (35) was performed on purified protein of all expressed recombinant CRBN–TBD proteins. These analyses revealed a 1:1 stoichiometric ratio of Zn^{2+} bound to the TBD recombinant protein (Fig. S4, *C–F*). Moreover, protein secondary structure consistent with proper folding was also evident using CD (data not shown). Both IF (Fig. 3, *D–G*) and ITC (Fig. 3 (*H–K*) and Fig. S5) analyses demonstrated similar K_D values at equilibrium for thalidomide and the immunomodulatory compounds tested in binding to WT, E377V, V388I, and E377V/V388I hmCRBN–TBD (Table 1) with no binding observed by phthalimide (Fig. S5, *I–L*), used as a negative control.

To assess the impact of binding pocket residues, Ala mutations of two residues were generated (Table 1) (7, 26, 27) to test the impact of hydrogen bond formation and hydrophobic interaction with Trp-380. The W380A mutation completely abolished ligand interactions. Although His-378 forms two hydrogen bonds with the glutarimide ring (Fig. 3*C*), mutating this residue to Ala did not impact binding. This suggests that the backbone carbonyl of H378A retains the hydrogen bond interaction with the NH group of the glutarimide ring. To further probe the role of His-378 side chain in immunomodulatory drug binding, we conducted a pH dependence study to measure the binding affinity of Len to CRBN–TBD by ITC. The K_D values measured at pH 4.5, 5.5, 6.5, and 7.5 are 21.4 ± 3, 23.7 ± 8, 23.8 ± 7, and 11.3 ± 2 μM, respectively. Thus, protonation and deprotonation of the His-378 imidazole group has no impact on immunomodulatory drug binding to the TBD.

N-terminal stabilization of CRBN–immunomodulatory compound interactions

Finally, we compared binding affinities of Len to CRBN–TBD and full-length CRBN–DDB1 protein complex using ITC to assess the impact of residues outside of the TBD. The full-length CRBN–DDB1 complex displayed a K_D value of 0.64 μM ± 0.24 μM (pH 7.0) (Fig. 4*A*). This affinity is similar to published data using a fluorescence polarization-based assay (32). Moreover, these results are consistent with a single binding site within the protein complex. To gain more insight into immunomodulatory compound binding to CRBN–TBD, we synthesized *N*-methyl-Len as a negative control, where the *N*-methyl group of the glutarimide ring is predicted to cause steric hindrance in the binding pocket (Fig. S6) and lacks the key hydrogen bond donor to His-378. As expected, *N*-methyl-Len did not bind to either the CRBN–TBD or CRBN–DDB1 complex (Fig. 4*B*), as measured by ITC, indicating that the complex–drug interaction is mediated predominantly by the glutarimide binding pocket of the TBD. Interestingly, the binding affinity of Len to the CRBN–TBD is about 30-fold lower than the full-length CRBN–DDB1 complex. Moreover, full-length CRBN and CRBN–TBD have endothermic and exothermic reactions, respectively. Therefore, residues in the full-length protein appear to augment protein-ligand interactions in the binding pocket.

Acquired ubiquitin-proximity ligation in mouse cells establishes conserved ligase functions of mouse and human CRBN variants

The substrate-recruiting function of CRBN was then investigated using dBET1, which maintains the CRBN–TBD targeting domain but switches the substrate-recruitment domain to recognize BRD4 and other JQ1-associated targets (21). Using IF (Fig. 5*A*), the saturation binding curves for dBET1 are similar to that of Len, whereas, as expected, JQ1 alone does not bind to the CRBN–TBD. The structures of dBET1 and *N*-methyl-dBET1 (used as a negative control, based on the results of *N*-methyl-Len) are provided in Fig. 5*B* to show the CRBN- and BET-targeting groups. Moreover, *N*-methyl-dBET1 confirms that this analog is interacting with similar residues in the TBD. Next, the function of dBET1 in activated human T cells was assessed, and results are shown in Fig. 5 (*C–G*); statistical analysis is provided in Table S3. Unlike Len and Pom, which activate T cells, BRD4 and c-Myc inhibition is expected to induce cell death or functionally repress these cells, as they are critical mediators of T-cell proliferation and survival (36, 37). Relative viability of activated T cells is reduced by dBET1 treatment compared with

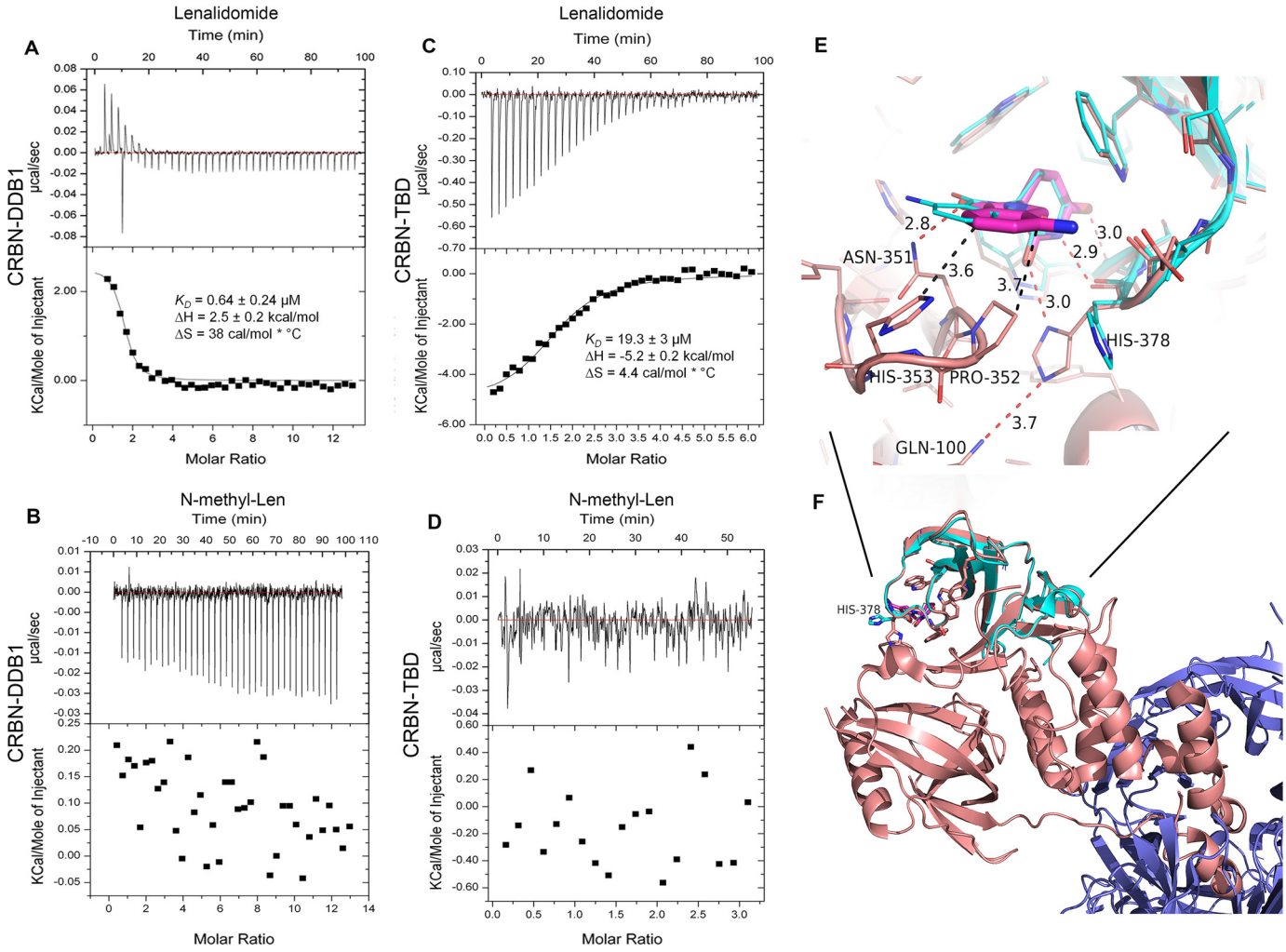

Figure 4. Lenalidomide binds to the TBD and CRBN–DDB1 protein complex. ITC binding curves of lenalidomide (*A* and *C*) and *N*-methyl-lenalidomide (*B* and *D*) titrated with CRBN–DDB1 complex (*A* and *B*) and CRBN–TBD (*C* and *D*). *E* and *F*, *schematic view* of lenalidomide interaction in the binding pocket of full-length human cereblon; human full-length CRBN (*salmon*) and DDB1 (*blue*) with bound lenalidomide (*magenta*) (PDB code 5FQD) superimposed with mouse TBD-CRBN (*cyan*) (PDB code 4TZU). Hydrogen bonds and hydrophobic interactions are shown in *red* and *black dashed lines*, respectively (see also Fig. S6). Data in figure represent mean ± S.D.

DMSO and is more active relative to treatment with increasing doses of JQ1 (Fig. 5*C*), suggesting that growth suppression by the heterobifunctional conjugate is superior to JQ1, as shown previously in leukemia cells (21). Importantly, decreased BRD4 protein expression is only evident with dBET1 treatment, whereas both dBET1 and JQ1 suppress the activation of c-Myc protein expression by Western blot analysis (Fig. 5*D*) and flow cytometry (Fig. 5*E*; summary of data in Fig. 5*F*), as expected, through BRD4 functional repression. Notably, the effect on BRD4 is reversed by incubation with *N*-methyl-dBET1 at doses of 0.1–10 μM. Repression of c-Myc at very high doses of *N*-methyl-dBET1 is consistent with activity of the JQ1-targeting molecule (Fig. 5, *D* and *F*). From these results, we conclude that human T cells respond to dBET1 through interactions that are mediated by the hydrophobic pocket of the CRBN–TBD. Finally, the suppressive effects observed with dBET1 treatment shows that the CRBN-targeting molecule in this compound is no longer activating IL-2, as shown in Len and Pom (Fig. 5*G*).

Next, saturation binding curves of V388I-TBD mutant titrated with Len (K_D = 15.6 ± 2.2 μM), dBET1 (K_D = 26.0 ± 2.1 μM), and *N*-methyl-dBET1 (nonbinding control) show that the mode and binding affinity of dBET1 are similar to those of the human-TBD protein (Table 1 and Fig. 6*A*). Mouse T cells were purified from $Crbn^{+/+}$ and $Crbn^{-/-}$ mice and used to evaluate the role of mouse CRBN in BRD4 degradation (Fig. 6, *B* and *C*), activation-induced proliferation, viability, and c-Myc and CD98 (Myc target gene) (Fig. 6, *D–G*) expression in response to dBET1 treatment (Fig. 5*B*). TCR stimulation with anti-CD3ϵ + anti-CD28 is required for the induction of c-*myc* in primary mouse T cells (data not shown). Both JQ1 and dBET1 suppressed c-Myc in activated T cells, but the reduction in protein expression of BRD4 was only observed after dBET1 treatment in $Crbn^{+/+}$ mouse T cells, consistent with proteasome engagement (Fig. 6*B*) through a CRBN-dependent mechanism. Pomalidomide treatment failed to impact BRD4 expression and further supports redirection of CRBN's ubiquitin-conjugating function through JQ1. To assess whether dBET1 is interacting directly with the TBD of mouse CRBN *in vivo*, an assay was performed using mouse $Crbn^{+/+}$ T cells treated with Pom in the presence and absence of dBET1. Results shown in

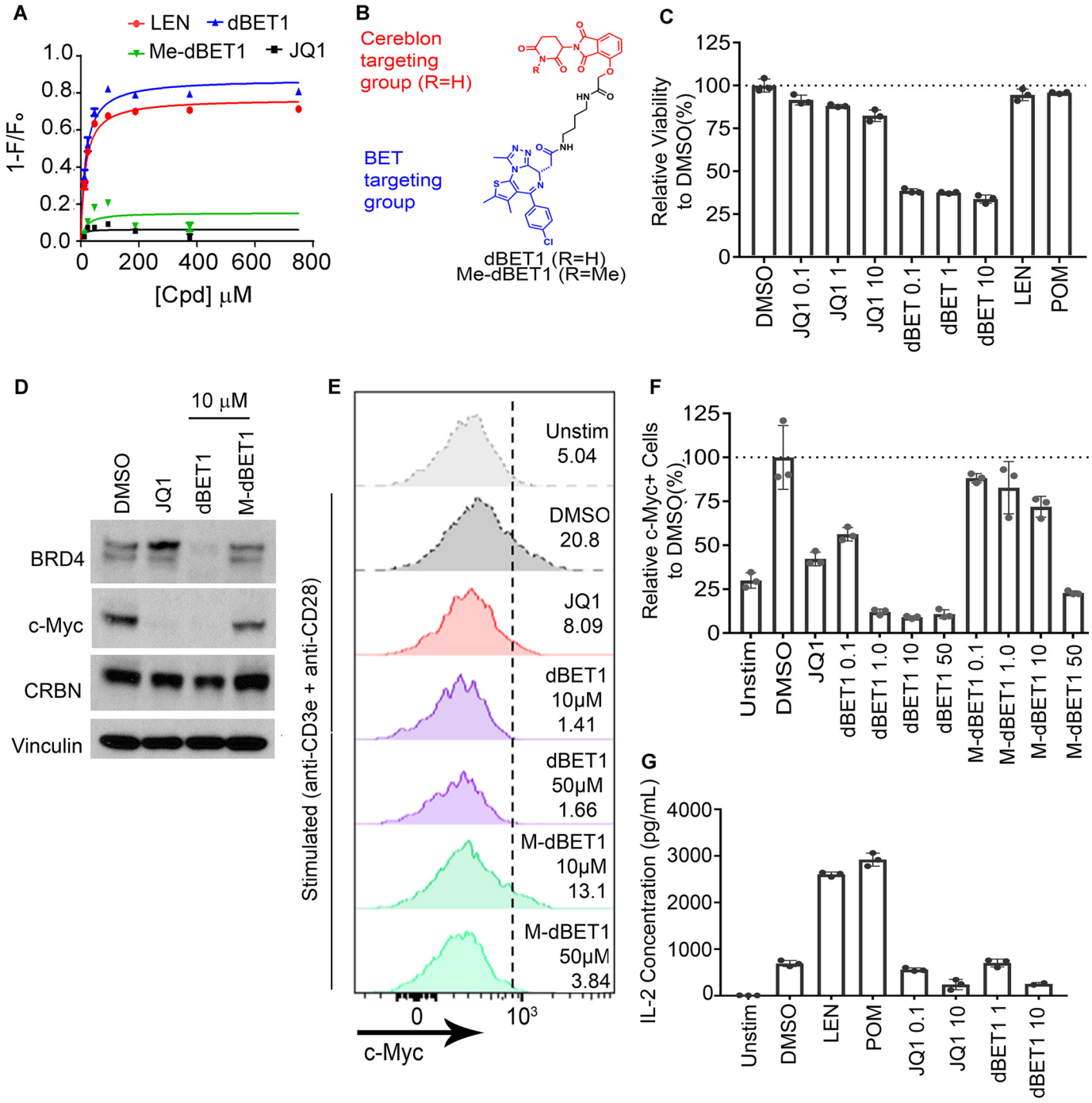

Figure 5. Functional activity of lenalidomide, JQ1, and dBET1 in human T cells and binding affinities of JQ1, dBET1, and Len to human CRBN. *A*, saturation binding curves of human TBD WT titrated with lenalidomide (K_D = 15.6 ± 2.2), JQ1 (no binding), dBET1 (K_D = 26.0 ± 2.1), and *N*-methyl-dBET1 (no binding) by fluorescence assay (see also Table 1 for a summary of all K_D values). *B*, structure of dBET1 and *N*-methyl-dBET1. *C*, human T cells purified from peripheral blood mononuclear cells from healthy donors and stimulated with anti-CD3ϵ/CD28. At the time of TCR stimulation, DMSO (vehicle control), the indicated concentrations of JQ1 and dBET1, 10 μM Len, and 10 μM Pom were added to the cell cultures. Cell viability was determined after 72 h by flow cytometry using Zombie NIR™ staining. *D*, Western blot analysis for expression of BRD4, CRBN, c-Myc, and vinculin in human T cells stimulated with anti-CD3ϵ/CD28 and treated simultaneously with vehicle (DMSO, 0.1%), JQ1, dBET1 (10 μM), and *N*-methyl-dBET1 (10 μM) for 48 h. Unstimulated cells are not shown in *D*. *E*, c-Myc expression by flow cytometry (histogram data) is shown following 48-h stimulation with anti-CD3ϵ/CD28. Drug treatments and doses are indicated. Expression of c-Myc requires stimulation based on comparison with unstimulated cells (*unstim*). Values represent percent positive relative to unstimulated cells based on gate (*dotted line*). *F*, quantification of flow data shown in *E* represented as percentage of DMSO. *Bar height* is the mean of individual values shown representative of three independent experiments. *Error bars*, S.D. from an exemplary experiment. *G*, unstimulated (*unstim*) or anti-CD3ϵ/CD28–stimulated T cells were treated with 10 μM Len, 10 μM Pom, and the indicated doses of JQ1 or dBET1. ELISAs were used to quantify IL-2 concentrations (pg/ml) from supernatants harvested at 48 h. Results shown are representative of three independent experiments. *Bar height*, mean of individual values; *error bars*, S.D. from an exemplary experiment. Results of statistical analysis are provided in Table S3.

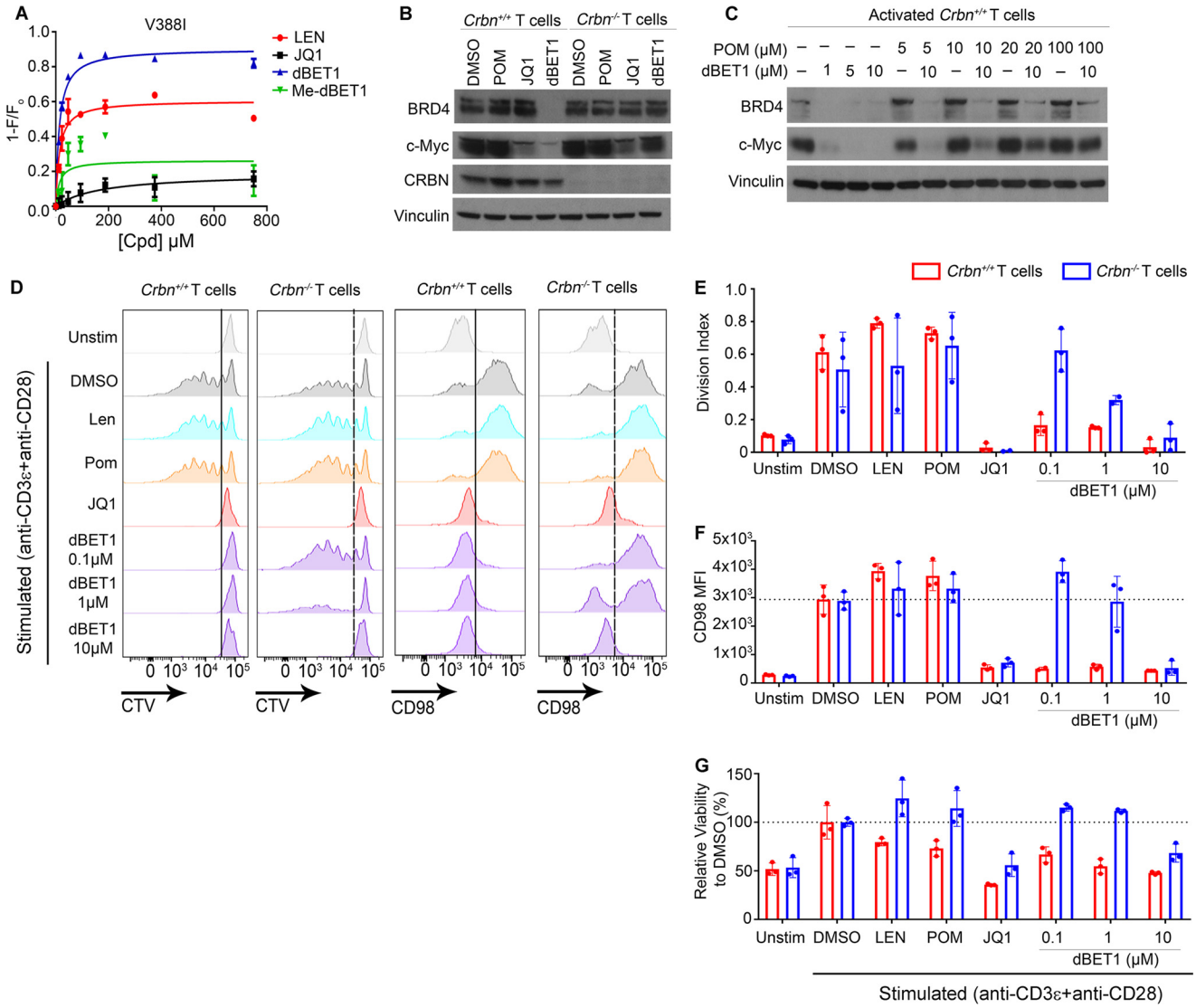

Figure 6. Functional activity of lenalidomide, pomalidomide, JQ1, and dBET1 in mouse T cells. *A*, saturation binding curves of human V388I mutant TBD titrated with lenalidomide ($K_D = 18 \pm 4$), JQ1 (no binding), dBET1 ($K_D = 18 \pm 3$), and *N*-methyl-dBET1 (no binding) by fluorescence assay (see also Table 1). *B*, mouse T cells purified from spleens of C57BL/6j mice with homozygous deletion of *Crbn* and WT littermates were stimulated with anti-CD3ϵ/CD28 in the presence of 0.1% DMSO (vehicle control), 10 μM Pom, 10 μM JQ1, or 10 μM dBET1. Western blots for BRD4, c-Myc, CRBN, and vinculin (loading control) expression are shown. *C*, Western blot analysis showing expression of BRD4, c-Myc, and vinculin from $Crbn^{+/+}$ T cells stimulated with anti-CD3ϵ/CD28 for 12 h with the indicated doses of dBET1, Pom, or combined treatment. *D*, purified $Crbn^{+/+}$ and $Crbn^{-/-}$ mouse T cells stimulated with anti-CD3ϵ/CD28 and treated with 0.1% DMSO (vehicle control), 10 μM Len, 10 μM Pom, 10 μM JQ1, or increasing doses of dBET1 for 72 h. Histogram plots from one experiment show proliferation (determined by dilution of CTV) and CD98 expression of T cells. *E*, proliferation index based on CTV data was used to calculate the amount of proliferation using an algorithm available with Flowjo analysis software (Tree Star). *F*, expression of CD98 was calculated relative to unstimulated cells using gates shown based on mean fluorescence intensities (*MFI*) of T cells as shown in *D*. *G*, cell viability was determined after 72 h by flow cytometry using Zombie NIR™ staining. Results shown are representative of three independent experiments. *Bar height* represents mean of individual values, and *error bars* represent S.D. from an exemplary experiment. Results of statistical analysis are provided in Table S4.

Fig. 6*C* show that at high concentrations of Pom (10-fold excess), the impact of dBET1 on c-Myc and BRD4 expression was reversed, suggesting that dBET1 is directly engaging the TBD of mouse CRBN. We next examined proliferation (*i.e.* division index) measured by dilution of cell trace violet (CTV) using methods described previously (38), expression of a c-Myc target gene (CD98), and viability using flow cytometry (Fig. 6*D*). Histograms (Fig. 6*D*) and summarized results (Fig. 6, *E–G*) show that the division index (based on CTV data) and CD98 expression (median fluoresce intensity (*MFI*)) are induced through activation (unstimulated *versus* DMSO) and that there is a differential response to dBET1 treatment in $Crbn^{+/+}$ and $Crbn^{-/-}$ T cells at 0.1 and 1 μM. The suppression of T cells at 10 μM is probably related to the JQ1-targeting molecule, because proliferation, c-Myc–regulated CD98 expression, and viability were suppressed independently of CRBN expression. Moreover, BRD4 degradation by dBET1 is similar in MM1.S human and 5TGM1 mouse multiple myeloma cells, confirming the conserved ubiquitin-conjugating functions of CRBN (Fig. S7).

Discussion

CRBN was first identified in mild autosomal recessive nonsyndromic intellectual disability (39) but has poorly defined physiological functions. Interactions have been reported with

the AMP-activated protein kinase α1 subunit (40), TAK1–TRAF6 (41), and CD147–MCT1 complex (42), where CRBN plays ubiquitin-independent roles in pathway regulation. The mechanistic underpinnings for induced limb deformities in chickens and zebrafish, but not in mice, appears dependent on sequence differences in mouse CRBN (20), which brings into question whether these differences in CRBN render it functionally inactive. Although reference CRBN sequences for nearly all examined primates possess Val-388, according to the Exome Aggregation Consortium, the Ile-391 variant occurs in humans at a frequency of 0.005% (rs756414303). Our data show that mutating Val-388 to Ile (V388I) does not alter binding affinity to the immunomodulatory compounds, suggesting that the contact between the immunomodulatory drug and the CRBN–TBD is maintained and potentially functionally active.

When bound to immunomodulatory drugs (Len, Pom, and CC-122), CRBN induces the destruction of three substrates, Ikaros, Aiolos, and CK1α (13), via a Val-388 interaction (1). In T cells, the IKZF-family transcription factors repress *IL2* so that ubiquitin-mediated destruction may be responsible for promoting T cell activation (13, 16). Our data solidify the mechanistic involvement of CRBN Ile-391 in drug resistance in mouse cell lines, as suggested previously by the finding that overexpression of *hCRBN* with Val-388, but not Ile-391, in Ba/F3 cells was sufficient to restore Ikaros protein destruction (13, 20).

As expected, using dBET1, there was no Ikaros degradation in mouse T cells or mouse myeloma cell lines. However, we found that dBET1 impressively reduced the expression of BRD4 in both human and mouse cells. Therefore, proximity-associated ubiquitin-conjugating functions of mouse and human CRBN are confirmed using dBET1. $Crbn^{-/-}$ T cells demonstrated that dBET1 functions through a CRBN–TBD–dependent process. Competition with Pom further suggests that the TBD of human and mouse CRBN have similar binding modes for immunomodulatory compounds, suggesting that there is both structural and functional conservation. Thus, the endogenous E3 ubiquitin ligase activity and assembly of the CRBN–DDB1–CUL4A–containing complex are fundamentally conserved across the vertebrate lineage, including the mouse, and probably other species, expressing Ile-391. Moreover, other sequence variants present in mouse CRBN, including difference in the N terminus, fail to impact its substrate-recruiting functions when targeting BRD4. This observation, along with the high degree of CRBN conservation, indicates that selective pressure has maintained the overall structure and function in CRBN for over 400 million years.

Using ITC and fluorescence-based binding assays, we establish that the dissociation constants of thalidomide and other immunomodulatory compounds to mouse CRBN are similar to human CRBN, which is consistent with analysis of the crystal structure of human CRBN–DDB1 in complex with Len (32, 33). As suggested previously (32), the W380A mutant completely abolished binding, which confirms that this is one of the key residues of the binding pocket. Trp-380 also appears to work synergistically with other binding pocket residues (Trp-386, Trp-400, and Phe-402) for ligand interaction. The K_D values of immunomodulatory compounds in complex with the human TBD (amino acids 319–425) are in the micromolar range, similar to those of *Caenorhabditis elegans* and *Magnetospirillum gryphiswaldense* (43). Based on the conserved CRBN structure, we synthesized *N*-methyl derivatives of Len and dBET1, which proved useful in assessing the functional contribution of this ligand interaction *in vivo* in mouse and human cells.

Here, we show an interesting reliance of the rigid TBD-binding pocket on N-terminal sequences, which plays a previously unappreciated role in optimal ligand binding. A conformational change in full-length CRBN–DDB1 may occur upon ligand binding, as shown by the difference in their ΔH and ΔS values (Fig. 4). Notably, the CRBN–DDB1 complex and CRBN–TBD show a marked difference in Len-binding affinity by ITC. In fact, a closer inspection of the crystal structure of full-length CRBN in complex with Len illustrates that a disordered loop in the TBD consisting of residues Asn-351, Pro-352, and His-353 stabilizes the interaction of Len. Asn-351 forms a hydrogen bond to a carbonyl oxygen of Len's isoindolinone ring, and both Pro-352 and His-353 form hydrophobic interactions with the aromatic system of the immunomodulatory drug (Fig. 4*E*). Importantly, the mouse TBD crystal structure shows poor electron density in this loop structure, suggesting that it is a highly unstructured and dynamic region. Alternatively, other residues outside the TBD could have stabilized this loop. The side chain of Gln-100, which is located in the LON domain of CRBN, forms a weak hydrogen bond interaction to the ϵ^2NH group of His-378. This in turn positions the δ^1NH of His-378 as a hydrogen donor to the immunomodulatory drugs. These important structural domains should be further investigated in immunomodulatory drug discovery.

Collectively, our results suggest that PROTAC molecules and possibly other CRBN-bound compounds may adopt an active conformation that is susceptible to CRBN-directed, cullin–RING E3 ligase–mediated polyubiquitination in mouse cells. PROTAC molecules are designed to harness the CRBN-binding properties of IMiDs and initiate the degradation of oncogenic targets. Several IMiD-based BET-targeting PROTACs, such as dBET-1, ARV-825, and BETd-260 have been developed to potently degrade BRD4 (22, 44, 45). Intracellular protein degradation of FK506-binding protein (FKBP12) was also achieved by a conjugate of thalidomide (21, 46), but originally, methionine aminopeptidase-2 (MetAP-2) (25), estradiol, and dihydroxytestosterone were degraded by engaging the Skp1–Cullin–F-box (SCF) ubiquitin ligase through a 10-amino acid phosphopeptide derived from IκBα (23, 47). PROTAC with specificity for the von Hippel–Lindau ubiquitin ligase E3 have also been developed (48, 49). Recently, BRD4 and ERK1/2 degradation was induced by the interaction of two smaller precursors molecules that undergo intracellular self-assembly, which improves solubility and cellular permeability of thalidomide-containing PROTAC inhibitors (50). Importantly, our studies establish that mouse platforms can indeed be used for preclinical development of dBET1 and possibly other PROTAC-based chemical degraders that are designed to redirect CRBN's substrate-binding function toward specified endogenous proteins (21, 23, 25, 44, 50, 51). Toxicology and functional testing of such agents in rodents and mouse tumor models may yield important preclinical information.

Experimental procedures

Animals and cell lines

Germ line *Crbn*-deficient mice ($Crbn^{-/-}$) were described previously (39), and gene deletion was confirmed using WT and *Crbn*-KO–specific primers. C57BL/6 ($Crbn^{+/+}$) mice were purchased from Jackson Laboratory (Farmington, CT) and were then bred to $Crbn^{-/-}$ mice. $Crbn^{+/+}$ and $Crbn^{-/-}$ littermates from $Crbn^{+/-}$ intercrosses were used for our studies. Mice were maintained and bred at the H. Lee Moffitt Cancer Center and Research Institute under a protocol approved by the institutional animal care and use committee. The human multiple myeloma cells, including U266, H929, and MM1.S, and the mouse multiple myeloma cell line 5TGM1 were generous gifts of Drs. Ken Shain and Connor Lynch (Moffitt Cancer Center, Tampa, FL). All cell lines were mycoplasma-free and sequence-verified.

T-cell isolation, activation, and drug treatments

Human polyclonal $CD3^+$ T cells or $CD8^+$ T cells were isolated from peripheral blood donations to the Southwest Florida Blood Services. Because personal identifying information is unavailable, the research was deemed nonhuman research. Human and mouse T cells were isolated from $Crbn^{+/+}$ and $Crbn^{-/-}$ splenocytes by immunomagnetic negative selection (Miltenyi Biotec, San Diego, CA), and >95% purity was confirmed by flow cytometry. For drug treatment experiments, 12-well flat bottom plates were coated with 5 μg/ml anti-CD3ϵ (clone HIT3a (eBioscience) or clone (145-2C11)) in 1× PBS at 37 °C for 60 min. Cells were plated at $2–4 \times 10^6$ cells/well with anti-CD28 (clone CD28.2 (eBioscience) or clone 37.51 (eBioscience)). Following 12 h of activation, the cells were treated with DMSO (0.1%, Sigma-Aldrich), Len (10 μM) (Celgene, NJ), Pom (Sigma-Aldrich), and JQ1 (doses indicated) (catalog no. SML0974, Sigma-Aldrich). *N*-Methyl-Len, dBET1, and *N*-methyl-dBET1 were all synthesized at the Moffitt Cancer Center (described in the supporting material) and used at the doses indicated. After 12 h of drug treatment, cells were harvested, and protein levels were examined by Western blot analysis. For proliferation experiments using mouse T cells, 0.1–10 μg/ml anti-CD3ϵ (clone 145-2C11, eBioscience) was used with cells plated with and without anti-CD28 for 72 h. Cytokine expression was determined using supernatants that were harvested at 24 or 48 h and quantified from standard curves by ELISA according to the manufacturer's protocol. Kits were purchased from eBioscience (IL-2) and R&D Systems for other cytokines. For functional analysis of T cells treated with JQ1, murine $CD3^+$ T cells from $Crbn^{+/+}$ and $Crbn^{-/-}$ splenocytes and human T cells were labeled with 5–10 μM CellTrace Violet (C34557, Thermo Fisher Scientific) and activated with 5 μg/ml anti-CD3ϵ and 1 μg/ml anti-CD28 for 72 h in round-bottom 96-well plates. Cells were stained with CD98-PE (clone RL388, Biolegend), 7-aminoactinomycin D (BD Pharmingen), and the Zombie NIR™ fixable viability kit (catalog no. 423105, Biolegend) and analyzed on a BD LSRII flow cytometer.

Quantitative real-time PCR

Isolated T cells from $Crbn^{+/+}$ and $Crbn^{-/-}$ mice were lysed and homogenized (Qiashredder, Qiagen), and total RNA was extracted (RNeasy, Qiagen) according to the manufacturer's protocol. Complementary DNA was generated from isolated RNA (iScript cDNA synthesis kit, Bio-Rad). RNA expression was analyzed by quantitative real-time PCR using Taqman Universal PCR Master Mix for Taqman probes (Thermo Fisher Scientific) against (cDNA) c-Myc (Mm00487804_m1) and (cDNA) β2 M (Mm00437762_m1). Samples were run on an Applied Biosystems 7900 HT and Sequence Detection Systems software.

Treatment of multiple myeloma cells

Mouse and human multiple myeloma cell lines were plated at $2–4 \times 10^6$ cells/well in a 12-well plate with various concentrations of Len and Pom. To confirm target degradation, the cells were treated with varying concentrations of dBET1 (0, 0.01, 0.1, 1, and 10 μM) for 12–24 h. Following drug treatment, protein levels were examined by Western blot analysis relative to vinculin or β-actin to normalize for protein expression. For proliferation studies, $1–2 \times 10^4$ cells/well were seeded in a 96-well plate and were treated with using the CCK8 (cell-counting-8) kit (Dojindo, Rockville, MD) according to the manufacturer's protocol.

General chemistry information

All reagents were purchased from commercial suppliers and used without further purification (except where mentioned otherwise). ^{1}H NMR spectra were recorded on an Agilent-Varian Mercury 400-MHz spectrometer with DMSO-d_6 as the solvent. All coupling constants are measured in hertz, and the chemical shifts (δH) are quoted in parts per million relative to TMS (δ0), which was used as the internal standard. High-resolution MS was carried out on an Agilent 6210 LC-MS (electrospray ionization-TOF) system. HPLC analysis was performed using a JASCO HPLC system equipped with a PU-2089 Plus quaternary gradient pump and a UV-2075 Plus UV-visible detector, using an Alltech Kromasil C-18 column (150 × 4.6 mm, 5 μm) and an Agilent Eclipse XDB-C18 column (150 × 4.6 mm, 5 μm). The purities of the final compounds used for the biochemical and functional studies were >95% as measured by HPLC. Melting points were recorded on an Optimelt automated melting point system (Stanford Research Systems). TLC was performed using silica gel 60 F254 plates (Thermo Fisher Scientific), with observation under UV when necessary. Anhydrous dimethylformamide was used as purchased from Sigma-Aldrich. Burdick and Jackson HPLC-grade solvents were purchased from VWR for HPLC, HPLC-MS, and high-resolution mass analysis. dBET1 (HPLC purity 98%) was prepared from JQ1 as described (21). Detailed information about the synthesis of *N*-methyl-Len, and *N*-methyl-dBET1 synthesis are provided in the supporting material.

Cloning, protein expression, and purification

The full-length hCRBN protein (isoform 1) in complex with DDB1 was a generous gift from Celgene Corp. (San Diego, CA). The gene coding for the human TBD (amino acids 319–425)

was synthesized and subcloned into the BamHI-NotI restriction sites of the pGEX-6P-1 vector by GeneArt® gene synthesis. The gene was engineered with silent mutations that utilize the favored *E. coli* codons. TBD E377V, V388I, H378A, and W380A mutations were performed using PCR. Details of primer sequences are provided in the supporting material. Mutations were confirmed by sequencing. The recombinant DNA plasmids were transformed into *E. coli* Rosetta™ 2(DE3)pLysS competent cells (EMD Millipore, Billerica, MA) for subsequent protein expression. The GST-tagged TBD proteins linked with PreScission protease proteolytic site were expressed and purified as follows. A single colony of freshly transformed cells was cultured at 37 °C for 16 h in 5 ml of Luria–Bertani (Thermo Fisher Scientific) medium containing 100 μg/ml ampicillin (Sigma-Aldrich) and 34 μg/ml chloramphenicol (Sigma-Aldrich). 1 ml of the culture was then used to inoculate 25 ml of Terrific Broth–phosphate medium (Thermo Fisher Scientific) with 100 μg/ml ampicillin at 37 °C for 16 h. The culture was then transferred to 1.5 liters of Terrific Broth–phosphate medium supplemented with 50 μM $ZnCl_2$ (Sigma-Aldrich). The resultant culture was incubated with continuous shaking at 250 rpm to an A_{600} of 0.70 and then induced with isopropyl-β-D-thiogalactopyranoside (0.5 mM final concentration; Thermo Fisher Scientific) at 16 °C for 20 h before harvesting by centrifugation at 6000 rpm for 30 min. The cells were lysed by homogenization in 50 mM Tris (pH 8.0; Sigma-Aldrich), 500 mM NaCl (Thermo Fisher Scientific), 1 mM TCEP (Sigma-Aldrich), 0.1% Triton X-100 (Sigma-Aldrich), 10 μM $ZnCl_2$ (Acros Organics, Thermo Fisher Scientific), and protease inhibitor mixture (Roche Applied Science). The protein was then purified by affinity chromatography on an AKTA Explorer or AKTA Purifier (GE Healthcare Life Sciences) using a GSH-Sepharose matrix (GE Healthcare) pre-equilibrated with 50 mM Tris (pH 8.0), 500 mM NaCl, 1 mM TCEP, and 10 μM $ZnCl_2$ and eluted with the same buffer with the addition of 10 mM reduced GSH (Sigma-Aldrich). Purity of the protein in the different fractions was determined by SDS-PAGE, and the best fractions were pooled. GST was cleaved from the pooled GST-TBD fractions by digestion with PreScission protease at 4 °C for 4 h. GST was removed from the resultant digest by a second round of GST affinity chromatography. Proteins were further purified by size-exclusion chromatography in a Superdex 75 column (GE Healthcare Life Sciences). Fractions with >90% purity were pooled, concentrated by ultrafiltration (10K Amicon tubes, EMD Millipore), and stored at −80 °C.

Zincon assay

All chemicals used in this assay were purchased from Sigma-Aldrich. The assay was adapted from previously published methods (35). A zinc concentration standard curve was prepared in 50 mM borate buffer, pH 9.0, containing 4 M NaCl, 8 M urea, and 40 μM zincon (2-carboxy-2′-hydroxy-5′-sulfoformazylbenzene) dye. Purified proteins were acidified with 300 mM HCl to facilitate the release of the zinc ions bound to the protein. The protein polypeptide was separated from the water-soluble layer by centrifugation. The solution was then spiked with 10–20 μM zinc sulfate. Absorption spectra between 400 and 750 nm were recorded. λ_{max} of free zincon and zincon–zinc complex were measured at 480 and 620–630 nm, respectively. Absorbance at 630 nm of different zinc concentrations was used to generate the linear regression curve. The concentration of zinc-containing protein was extrapolated based on the linear regression curve.

ITC

The binding of CRBN–DDB1 complex and CRBN–TBD WT and mutant variants to immunomodulatory compounds was analyzed with a MicroCal iTC200 titration calorimeter (Malvern, Westborough, MA). The compound phthalimide was used as the negative control. The proteins were rebuffered into binding buffer (50 mM HEPES (pH 7.5, Sigma-Aldrich), 200 mM NaCl, 0.1 mM TCEP, and 0.6% DMSO). For the titrations of the protein constructs, a total of 19 aliquots (2.05 μl each) of the respective compounds (~600 μM) were injected into 200 μl of the protein solutions (40 μM) at 25 °C. The ITC cell mixture was constantly stirred at 1000 rpm and recorded for 160 s between injections at low feedback. The corrected heat values were fitted using a nonlinear least square curve-fitting algorithm (Microcal Origin version 7.0, OriginLab, Northampton, MA) to obtain binding constants (K_D) and values for n (number of binding sites), ΔH (enthalpy), and ΔS (entropy).

Intrinsic tryptophan fluorescence assay

Binding of compounds to WT and mutant TBD was monitored by fluorescence spectroscopy, using an adapted previously published method (14, 43). All chemicals used in this assay were purchased from Sigma-Aldrich unless otherwise stated. In this assay, changes in emission spectra are induced by interactions of these compounds with the three Trp residues (Trp-380, Trp-386, and Trp-400) in the binding site (32, 33). TBD proteins (final concentration, 10 μM) were incubated with varying final concentrations (0–750 μM) of compounds in assay buffer (50 mM Tris, pH 7.5, 200 mM NaCl, 0.1% Pluronic-F127, and 1 mM TCEP) to a final volume of 40 μl in a black 96-well half-area plate (Corning, Inc.). A 0.5% final DMSO concentration was used in each well. Samples were excited at 280 nm, and fluorescence emission intensities were measured at 340 nm using a Wallac Envision 2102 multilabel plate reader (Perkin-Elmer Life Sciences). All measurements were done in triplicate and corrected for inner filter effect to subtract for ligand-associated fluorescence, as described (52). The magnitude of fluorescence difference ($1 - F/F_0$) was measured, where F is the fluorescence emission at a given concentration of ligand; F_0 is the intrinsic fluorescence intensity of 10 μM TBD protein alone. Graph plotting and curve fitting to obtain apparent dissociation constant (K_D) values were calculated by fitting the relative change in intrinsic fluorescence at 340 nm ($1 - F/F_0$) *versus* ligand concentration to a nonlinear regression with one-site binding hyperbola with GraphPad Prism (GraphPad Software, La Jolla, CA).

Theoretical calculations

The preparation of the protein systems for hCRBN (PDB code 4TZ4 (32), mCRBN (PDB codes 4TZC and 4TZU) (32), and gCRBN (PDB codes 4CI1, 4CI2, and 4CI3) (33) were done using the Schrödinger software suite (Maestro, version 9.7,

Schrödinger, LLC, New York). Protein structure coordinates were downloaded from the PDB (53, 54) and prepared with the Protein Preparation Wizard (PrepWizard) in Maestro (Schrödinger Suite 2014-1 Protein Preparation Wizard; Epik version 2.7, Schrödinger; Impact version 6.2, Schrödinger; Prime version 3.5, Schrödinger) (55). Final system equilibration was determined by the observation of asymptotic behavior of the potential energy, RMSD, and Rg profiles and visual inspection of trajectories guided by root mean square fluctuation profiles (supporting material provides additional detailed settings). MD simulations were performed with the Desmond MD program with additional details provided in the supporting Materials and Methods (Desmond Molecular Dynamics System, version 3). After equilibration was determined, a hierarchical average linkage clustering method based on RMSD was utilized to determine an average representative structure for each equilibrated system. The program PROPKA was then implemented again on the equilibrated structures to test the consistency of side chain protonation states at pH 7.4 (supporting Materials and Methods provides details for characterization of the ionization states for certain side chains).

Author contributions—A. A. A., A. Y. A., and R. M. contributed equally to the manuscript and designed the research, performed experiments, analyzed and interpreted data, prepared figures, and wrote the manuscript. M. S. B. performed experiments. A. B. designed the research plan, performed experiments, analyzed and interpreted data, and prepared the paper. J. M. M. performed experiments and analyzed and interpreted data. R. S. H. performed experiments, analyzed and interpreted data, and reviewed the paper. W. E. G. performed experiments, analyzed data, and prepared figures. S. G. designed the research, performed experiments, analyzed and interpreted data, and prepared figures. M. A. synthesized chemicals. Y. Y. produced protein for the project. M. R. K. performed experiments. M. E. O. conducted experiments. K. D. provided concept development for modeling, established experimental methods, and prepared the paper. W. G. provided concept development and provided expertise for modeling. J. A. Y. provided concept development and prepared the manuscript. A. M. R. provided critical reagents. E. S. provided assistance with experimental design, interpreted data, and prepared the paper. H. R. L. provided concept design for key reagents, interpreted results, and prepared the paper. N. J. L. and P. K. E. -B. shared equally in manuscript preparation and designed the research plan, performed data analysis and interpreted the results, prepared the paper, and were responsible for all aspects of the work.

Acknowledgments—hCRBN–DDB1 protein complex and the anti-CRBN antibody were generous gifts from Celgene Corp. (San Diego, CA). Multiple myeloma cell lines were provided by Drs. Kenneth Shain and Connor Lynch (Moffitt Cancer Center). We also thank John Cleveland, Ph.D. (Moffitt Cancer Center) for his expert opinion and assistance with manuscript preparation. The Chemical Biology Core Facility at the H. Lee Moffitt Cancer Center and Research Institute, is an NCI (National Institutes of Health)-designated Comprehensive Cancer Center (Grant P30-CA076292).

References

1. Krönke, J., Udeshi, N. D., Narla, A., Grauman, P., Hurst, S. N., McConkey, M., Svinkina, T., Heckl, D., Comer, E., Li, X., Ciarlo, C., Hartman, E., Munshi, N., Schenone, M., Schreiber, S. L., *et al.* (2014) Lenalidomide causes selective degradation of IKZF1 and IKZF3 in multiple myeloma cells. *Science* **343,** 301–305 CrossRef Medline
2. Bjorklund, C. C., Lu, L., Kang, J., Hagner, P. R., Havens, C. G., Amatangelo, M., Wang, M., Ren, Y., Couto, S., Breider, M., Ning, Y., Gandhi, A. K., Daniel, T. O., Chopra, R., Klippel, A., and Thakurta, A. G. (2015) Rate of CRL4(CRBN) substrate Ikaros and Aiolos degradation underlies differential activity of lenalidomide and pomalidomide in multiple myeloma cells by regulation of c-Myc and IRF4. *Blood Cancer J.* **5,** e354 CrossRef Medline
3. Ito, T., Ando, H., Suzuki, T., Ogura, T., Hotta, K., Imamura, Y., Yamaguchi, Y., and Handa, H. (2010) Identification of a primary target of thalidomide teratogenicity. *Science* **327,** 1345–1350 CrossRef Medline
4. Diggle, G. E. (2001) Thalidomide: 40 years on. *Int. J. Clin. Pract.* **55,** 627–631 Medline
5. Singhal, S., Mehta, J., Desikan, R., Ayers, D., Roberson, P., Eddlemon, P., Munshi, N., Anaissie, E., Wilson, C., Dhodapkar, M., Zeddis, J., and Barlogie, B. (1999) Antitumor activity of thalidomide in refractory multiple myeloma. *N. Engl. J. Med.* **341,** 1565–1571 CrossRef Medline
6. List, A., Kurtin, S., Roe, D. J., Buresh, A., Mahadevan, D., Fuchs, D., Rimsza, L., Heaton, R., Knight, R., and Zeldis, J. B. (2005) Efficacy of lenalidomide in myelodysplastic syndromes. *N. Engl. J. Med.* **352,** 549–557 CrossRef Medline
7. Robak, T., Blonski, J. Z., and Robak, P. (2016) Antibody therapy alone and in combination with targeted drugs in chronic lymphocytic leukemia. *Semin. Oncol.* **43,** 280–290 CrossRef Medline
8. Arora, M., Gowda, S., and Tuscano, J. (2016) A comprehensive review of lenalidomide in B-cell non-Hodgkin lymphoma. *Ther. Adv. Hematol.* **7,** 209–221 CrossRef Medline
9. Zeldis, J. B., Williams, B. A., Thomas, S. D., and Elsayed, M. E. (1999) S.T.E.P.S.: a comprehensive program for controlling and monitoring access to thalidomide. *Clin. Ther.* **21,** 319–330 CrossRef Medline
10. Gopalakrishnan, R., Matta, H., Tolani, B., Triche, T., Jr., and Chaudhary, P. M. (2016) Immunomodulatory drugs target IKZF1-IRF4-MYC axis in primary effusion lymphoma in a cereblon-dependent manner and display synergistic cytotoxicity with BRD4 inhibitors. *Oncogene* **35,** 1797–1810 CrossRef Medline
11. Fionda, C., Abruzzese, M. P., Zingoni, A., Cecere, F., Vulpis, E., Peruzzi, G., Soriani, A., Molfetta, R., Paolini, R., Ricciardi, M. R., Petrucci, M. T., Santoni, A., and Cippitelli, M. (2015) The IMiDs targets IKZF-1/3 and IRF4 as novel negative regulators of NK cell-activating ligands expression in multiple myeloma. *Oncotarget* **6,** 23609–23630 Medline
12. Fang, J., Liu, X., Bolanos, L., Barker, B., Rigolino, C., Cortelezzi, A., Oliva, E. N., Cuzzola, M., Grimes, H. L., Fontanillo, C., Komurov, K., MacBeth, K., and Starczynowski, D. T. (2016) A calcium- and calpain-dependent pathway determines the response to lenalidomide in myelodysplastic syndromes. *Nat. Med.* **22,** 727–734 CrossRef Medline
13. Krönke, J., Fink, E. C., Hollenbach, P. W., MacBeth, K. J., Hurst, S. N., Udeshi, N. D., Chamberlain, P. P., Mani, D. R., Man, H. W., Gandhi, A. K., Svinkina, T., Schneider, R. K., McConkey, M., Järås, M., Griffiths, E., *et al.* (2015) Lenalidomide induces ubiquitination and degradation of CK1α in del(5q) MDS. *Nature* **523,** 183–188 CrossRef Medline
14. Hagner, P. R., Man, H. W., Fontanillo, C., Wang, M., Couto, S., Breider, M., Bjorklund, C., Havens, C. G., Lu, G., Rychak, E., Raymon, H., Narla, R. K., Barnes, L., Khambatta, G., Chiu, H., *et al.* (2015) CC-122, a pleiotropic pathway modifier, mimics an interferon response and has antitumor activity in DLBCL. *Blood* **126,** 779–789 CrossRef Medline
15. Gandhi, A. K., Kang, J., Havens, C. G., Conklin, T., Ning, Y., Wu, L., Ito, T., Ando, H., Waldman, M. F., Thakurta, A., Klippel, A., Handa, H., Daniel, T. O., Schafer, P. H., and Chopra, R. (2014) Immunomodulatory agents lenalidomide and pomalidomide co-stimulate T cells by inducing degradation of T cell repressors Ikaros and Aiolos via modulation of the E3 ubiquitin ligase complex CRL4(CRBN). *Br. J. Haematol.* **164,** 811–821 CrossRef Medline
16. O'Brien, S., Thomas, R. M., Wertheim, G. B., Zhang, F., Shen, H., and Wells, A. D. (2014) Ikaros imposes a barrier to $CD8^+$ T cell differentiation by restricting autocrine IL-2 production. *J. Immunol.* **192,** 5118–5129 CrossRef Medline
17. Thomas, R. M., Chunder, N., Chen, C., Umetsu, S. E., Winandy, S., and Wells, A. D. (2007) Ikaros enforces the costimulatory requirement for IL2

gene expression and is required for anergy induction in CD4$^+$ T lymphocytes. *J. Immunol.* **179,** 7305–7315 CrossRef Medline
18. Chesi, M., Matthews, G. M., Garbitt, V. M., Palmer, S. E., Shortt, J., Lefebure, M., Stewart, A. K., Johnstone, R. W., and Bergsagel, P. L. (2012) Drug response in a genetically engineered mouse model of multiple myeloma is predictive of clinical efficacy. *Blood* **120,** 376–385 CrossRef Medline
19. Fratta, I. D., Sigg, E. B., and Maiorana, K. (1965) Teratogenic effects of thalidomide in rabbits, rats, hamsters, and mice. *Toxicol. Appl. Pharmacol.* **7,** 268–286 CrossRef Medline
20. Petzold, G., Fischer, E. S., and Thomä, N. H. (2016) Structural basis of lenalidomide-induced CK1α degradation by the CRL4 ubiquitin ligase. *Nature* **532,** 127–130 CrossRef Medline
21. Winter, G. E., Buckley, D. L., Paulk, J., Roberts, J. M., Souza, A., Dhe-Paganon, S., and Bradner, J. E. (2015) Drug Development: phthalimide conjugation as a strategy for *in vivo* target protein degradation. *Science* **348,** 1376–1381 CrossRef Medline
22. Lu, J., Qian, Y., Altieri, M., Dong, H., Wang, J., Raina, K., Hines, J., Winkler, J. D., Crew, A. P., Coleman, K., and Crews, C. M. (2015) Hijacking the E3 ubiquitin ligase cereblon to efficiently target BRD4. *Chem. Biol.* **22,** 755–763 CrossRef Medline
23. Sakamoto, K. M., Kim, K. B., Verma, R., Ransick, A., Stein, B., Crews, C. M., and Deshaies, R. J. (2003) Development of Protacs to target cancer-promoting proteins for ubiquitination and degradation. *Mol. Cell. Proteomics* **2,** 1350–1358 CrossRef Medline
24. Sakamoto, K. M. (2010) Protacs for treatment of cancer. *Pediatr. Res.* **67,** 505–508 CrossRef Medline
25. Sakamoto, K. M., Kim, K. B., Kumagai, A., Mercurio, F., Crews, C. M., and Deshaies, R. J. (2001) Protacs: chimeric molecules that target proteins to the Skp1-Cullin-F box complex for ubiquitination and degradation. *Proc. Natl. Acad. Sci. U.S.A.* **98,** 8554–8559 CrossRef Medline
26. Sievers, F., and Higgins, D. G. (2014) Clustal Omega, accurate alignment of very large numbers of sequences. *Methods Mol. Biol.* **1079,** 105–116 CrossRef Medline
27. Lindner, S., and Krönke, J. (2016) The molecular mechanism of thalidomide analogs in hematologic malignancies. *J. Mol. Med.* **94,** 1327–1334 CrossRef Medline
28. Lopez-Girona, A., Mendy, D., Ito, T., Miller, K., Gandhi, A. K., Kang, J., Karasawa, S., Carmel, G., Jackson, P., Abbasian, M., Mahmoudi, A., Cathers, B., Rychak, E., Gaidarova, S., Chen, R., *et al.* (2012) Cereblon is a direct protein target for immunomodulatory and antiproliferative activities of lenalidomide and pomalidomide. *Leukemia* **26,** 2326–2335 CrossRef Medline
29. Otáhal, P., Prková, D., Král, V., Fabry, M., Vočková, P., Latečková, L., Trněný, M., and Klener, P. (2016) Lenalidomide enhances antitumor functions of chimeric antigen receptor modified T cells. *Oncoimmunology* **5,** e1115940 CrossRef Medline
30. McDaniel, J. M., Zou, J. X., Fulp, W., Chen, D. T., List, A. F., and Epling-Burnette, P. K. (2012) Reversal of T-cell tolerance in myelodysplastic syndrome through lenalidomide immune modulation. *Leukemia* **26,** 1425–1429 CrossRef Medline
31. Gandhi, A. K., Mendy, D., Waldman, M., Chen, G., Rychak, E., Miller, K., Gaidarova, S., Ren, Y., Wang, M., Breider, M., Carmel, G., Mahmoudi, A., Jackson, P., Abbasian, M., Cathers, B. E., *et al.* (2014) Measuring cereblon as a biomarker of response or resistance to lenalidomide and pomalidomide requires use of standardized reagents and understanding of gene complexity. *Br. J. Haematol.* **164,** 233–244 CrossRef Medline
32. Chamberlain, P. P., Lopez-Girona, A., Miller, K., Carmel, G., Pagarigan, B., Chie-Leon, B., Rychak, E., Corral, L. G., Ren, Y. J., Wang, M., Riley, M., Delker, S. L., Ito, T., Ando, H., Mori, T., *et al.* (2014) Structure of the human Cereblon-DDB1-lenalidomide complex reveals basis for responsiveness to thalidomide analogs. *Nat. Struct. Mol. Biol.* **21,** 803–809 CrossRef Medline
33. Fischer, E. S., Böhm, K., Lydeard, J. R., Yang, H., Stadler, M. B., Cavadini, S., Nagel, J., Serluca, F., Acker, V., Lingaraju, G. M., Tichkule, R. B., Schebesta, M., Forrester, W. C., Schirle, M., Hassiepen, U., *et al.* (2014) Structure of the DDB1-CRBN E3 ubiquitin ligase in complex with thalidomide. *Nature* **512,** 49–53 CrossRef Medline
34. Sherman, W., Beard, H. S., and Farid, R. (2006) Use of an induced fit receptor structure in virtual screening. *Chem. Biol. Drug Des.* **67,** 83–84 CrossRef Medline
35. Säbel, C. E., Neureuther, J. M., and Siemann, S. (2010) A spectrophotometric method for the determination of zinc, copper, and cobalt ions in metalloproteins using Zincon. *Anal. Biochem.* **397,** 218–226 CrossRef Medline
36. Wang, R., Dillon, C. P., Shi, L. Z., Milasta, S., Carter, R., Finkelstein, D., McCormick, L. L., Fitzgerald, P., Chi, H., Munger, J., and Green, D. R. (2011) The transcription factor Myc controls metabolic reprogramming upon T lymphocyte activation. *Immunity* **35,** 871–882 CrossRef Medline
37. Sun, Y., Wang, Y., Toubai, T., Oravecz-Wilson, K., Liu, C., Mathewson, N., Wu, J., Rossi, C., Cummings, E., Wu, D., Wang, S., and Reddy, P. (2015) BET bromodomain inhibition suppresses graft-versus-host disease after allogeneic bone marrow transplantation in mice. *Blood* **125,** 2724–2728 CrossRef Medline
38. Mailloux, A. W., Sugimori, C., Komrokji, R. S., Yang, L., Maciejewski, J. P., Sekeres, M. A., Paquette, R., Loughran, T. P., Jr., List, A. F., and Epling-Burnette, P. K. (2012) Expansion of effector memory regulatory T cells represents a novel prognostic factor in lower risk myelodysplastic syndrome. *J. Immunol.* **189,** 3198–3208 CrossRef Medline
39. Rajadhyaksha, A. M., Ra, S., Kishinevsky, S., Lee, A. S., Romanienko, P., DuBoff, M., Yang, C., Zupan, B., Byrne, M., Daruwalla, Z. R., Mark, W., Kosofsky, B. E., Toth, M., and Higgins, J. J. (2012) Behavioral characterization of cereblon forebrain-specific conditional null mice: a model for human non-syndromic intellectual disability. *Behav. Brain Res.* **226,** 428–434 CrossRef Medline
40. Lee, K. M., Jo, S., Kim, H., Lee, J., and Park, C. S. (2011) Functional modulation of AMP-activated protein kinase by cereblon. *Biochim. Biophys. Acta* **1813,** 448–455 CrossRef Medline
41. Min, Y., Wi, S. M., Kang, J. A., Yang, T., Park, C. S., Park, S. G., Chung, S., Shim, J. H., Chun, E., and Lee, K. Y. (2016) Cereblon negatively regulates TLR4 signaling through the attenuation of ubiquitination of TRAF6. *Cell Death Dis.* **7,** e2313 CrossRef Medline
42. Eichner, R., Heider, M., Fernández-Sáiz, V., van Bebber, F., Garz, A. K., Lemeer, S., Rudelius, M., Targosz, B. S., Jacobs, L., Knorn, A. M., Slawska, J., Platzbecker, U., Germing, U., Langer, C., Knop, S., *et al.* (2016) Immunomodulatory drugs disrupt the cereblon-CD147-MCT1 axis to exert antitumor activity and teratogenicity. *Nat. Med.* **22,** 735–743 CrossRef Medline
43. Hartmann, M. D., Boichenko, I., Coles, M., Zanini, F., Lupas, A. N., and Hernandez Alvarez, B. (2014) Thalidomide mimics uridine binding to an aromatic cage in cereblon. *J. Struct. Biol.* **188,** 225–232 CrossRef Medline
44. Saenz, D. T., Fiskus, W., Qian, Y., Manshouri, T., Rajapakshe, K., Raina, K., Coleman, K. G., Crew, A. P., Shen, A., Mill, C. P., Sun, B., Qiu, P., Kadia, T. M., Pemmaraju, N., DiNardo, C., *et al.* (2017) Novel BET protein proteolysis targeting chimera (BET-PROTAC) exerts superior lethal activity than bromodomain inhibitor (BETi) against post-myeloproliferative neoplasm (MPN) secondary (s) AML cells. *Leukemia* **31,** 1951–1961 CrossRef Medline
45. Zhou, B., Hu, J., Xu, F., Chen, Z., Bai, L., Fernandez-Salas, E., Lin, M., Liu, L., Yang, C. Y., Zhao, Y., McEachern, D., Przybranowski, S., Wen, B., Sun, D., and Wang, S. (2018) Discovery of a small-molecule degrader of bromodomain and extra-terminal (BET) proteins with picomolar cellular potencies and capable of achieving tumor regression. *J. Med. Chem.* **61,** 462–481 CrossRef Medline
46. Schneekloth, J. S., Jr, Fonseca, F. N., Koldobskiy, M., Mandal, A., Deshaies, R., Sakamoto, K., and Crews, C. M. (2004) Chemical genetic control of protein levels: selective *in vivo* targeted degradation. *J. Am. Chem. Soc.* **126,** 3748–3754 CrossRef Medline
47. Bargagna-Mohan, P., Baek, S. H., Lee, H., Kim, K., and Mohan, R. (2005) Use of PROTACS as molecular probes of angiogenesis. *Bioorg. Med. Chem. Lett.* **15,** 2724–2727 CrossRef Medline
48. Wang, X., Feng, S., Fan, J., Li, X., Wen, Q., and Luo, N. (2016) New strategy for renal fibrosis: targeting Smad3 proteins for ubiquitination and degradation. *Biochem. Pharmacol.* **116,** 200–209 CrossRef Medline
49. Zengerle, M., Chan, K. H., and Ciulli, A. (2015) Selective small molecule induced degradation of the BET bromodomain protein BRD4. *ACS Chem. Biol.* **10,** 1770–1777 CrossRef Medline

50. Lebraud, H., Wright, D. J., Johnson, C. N., and Heightman, T. D. (2016) Protein degradation by in-cell self-assembly of proteolysis targeting chimeras. *ACS Cent. Sci.* **2,** 927–934 CrossRef Medline
51. Raina, K., Lu, J., Qian, Y., Altieri, M., Gordon, D., Rossi, A. M., Wang, J., Chen, X., Dong, H., Siu, K., Winkler, J. D., Crew, A. P., Crews, C. M., and Coleman, K. G. (2016) PROTAC-induced BET protein degradation as a therapy for castration-resistant prostate cancer. *Proc. Natl. Acad. Sci. U.S.A.* **113,** 7124–7129 CrossRef Medline
52. Martin, M. P., Alam, R., Betzi, S., Ingles, D. J., Zhu, J. Y., and Schönbrunn, E. (2012) A novel approach to the discovery of small-molecule ligands of CDK2. *Chembiochem* **13,** 2128–2136 CrossRef Medline
53. Bernstein, F. C., Koetzle, T. F., Williams, G. J., Meyer, E. F., Jr., Brice, M. D., Rodgers, J. R., Kennard, O., Shimanouchi, T., and Tasumi, M. (1977) The Protein Data Bank: a computer-based archival file for macromolecular structures. *Eur. J. Biochem.* **80,** 319–324 CrossRef Medline
54. Berman, H. M., Westbrook, J., Feng, Z., Gilliland, G., Bhat, T. N., Weissig, H., Shindyalov, I. N., and Bourne, P. E. (2000) The Protein Data Bank. *Nucleic Acids Res.* **28,** 235–242 CrossRef Medline
55. Sastry, G. M., Adzhigirey, M., Day, T., Annabhimoju, R., and Sherman, W. (2013) Protein and ligand preparation: parameters, protocols, and influence on virtual screening enrichments. *J. Comput. Aided Mol. Des.* **27,** 221–234 CrossRef Medline